Low Temperature Physics ARTICLE scitation.org/journal/ltp

Quasiclassical calculations of Landau level spectrum for 20.5-nm-wide H gTe quantum well: "extremum loop" model and effects of cubic symmetry

Cite as: Fiz. Nizk. Temp. **47**, 11–17 (January 2021); doi: 10.1063/10.0002891
Submitted: 20 November 2020

S. V. Gudina,[1] A. S. Bogolubskiy,[1] V. N. Neverov,[1,a)] K. V. Turutkin,[1] N. G. Shelushinina,[1] and M. V. Yakunin[1,2]

AFFILIATIONS

[1]M. N. Miheev Institute of Metal Physics of the Ural Branch of the Russian Academy of Sciences, Ekaterinburg 620108, Russia
[2]Institute of Natural Sciences and Mathematics, Ural Federal University, Ekaterinburg 620002, Russia

[a)]**Author to whom correspondence should be addressed:** neverov@imp.uran.ru

ABSTRACT

Quasiclassical calculations of the effective cyclotron mass and the spectrum of Landau levels have been carried out for carriers of the size-quantized H2 subband with a nonmonotonic dispersion law, which forms a valence band of 20.5-nm-wide HgTe quantum well with an inverted band structure. The model of the so-called "extremum loop", previously developed by Rashba and Sheka for semiconductors with a wurtzite lattice, has been used for calculations. The results obtained are compared both with the empirical picture and with quantum-mechanical calculations of the Landau level spectrum for the HgTe quantum well in the semimetallic phase.

INTRODUCTION

In recent years, high-mobility HgTe-based heterostructures have become available for experimental investigations due to advances in the molecular beam epitaxy (MBE) technology (see, for example, Refs. 1 and 2 and references therein). At present, the study of magnetotransport, including the quantum Hall effect (QHE) regime, in HgTe /HgCdTe systems is an extensive and rapidly developing area of research.

A notable property of HgCdTe/HgTe/HgCdTe heterostructures is that, by varying the width of the HgTe quantum well (QW), transitions between the phases of a conventional (band) insulator, topological insulator, and semimetal can be achieved[1–8] (see, for example, Fig. 1 in Ref. 5). A clear physical model of the formation of size quantized subbands in a CdTe/HgTe/CdTe quantum well, based on information about the bulk structure of HgTe and CdTe, is presented in Ref. 1.

As the thickness of the HgTe layer increases, the material becomes more and more similar to bulk HgTe, and for wide QWs ($d_{QW} > d_C \approx 6.3$ nm) the spatially quantized energy spectrum of the HgTe layer is markedly specific due to its inversion character.

For $d_{QW} \gtrsim 8.3$ nm both the conduction and valence subbands built of the Γ_8-symmetry wave functions contrary to the traditional semiconductor structures with a conduction subband of the Γ_6 character.

In HgTe QW case, the first size-quantized heavy-hole subband H1 has an electronic character[9] and is a conduction band. The second size-quantized subband of heavy holes H2 with a non-monotonic dispersion law becomes the upper valence band.

Owing to a uniaxial strain of HgTe layer, which is caused by the lattice mismatch of HgTe and CdHgTe,[10] the energy spectrum of the H2 subband is essentially non-monotonic and has maxima away from the Γ point of the 2D Brillouin zone.

Moreover, the conduction subband may overlap here with the lateral maxima of the valence subband leading to the formation of a semimetal (SM) with coexisting electrons and holes. The overlap (and thus SM state) occurs in a relatively wide HgTe quantum wells (18–21 nm) with an inverted energy spectrum and various surface orientations (013), (112), and (100).[6–8]

Diverse new physics arises in such a semimetal. The picture of magnetic (Landau) levels in this semimetal is very intricate as it consists of two overlapped fan-charts oppositely directed in energy.[11–13]

In this paper, we present the results of semiclassical calculations of the cyclotron effective mass and the spectrum of the Landau levels (LL) of the QW HgTe valence band with an inverted band structure both in the isotropic approximation (the "extremum loop" model) and with the accounting for the effects of cubic symmetry. The semiclassical approach is important for the theoretical estimation of the effective mass of holes in a complex valence band with a non-monotonic dispersion law.

Numerical calculations of the effective mass of holes in the lateral maxima of the valence band (subband H2) for strong spectrum anisotropy (accounting for corrugation; asymmetry of the boundaries of a quantum well and differences in their smearing) in the quasiclassical approximation were performed in Ref. 14.

2. BAND STRUCTURE OF THE HGTE QUANTUM WELL AT B = 0

Band structure of HgTe/$Cd_{0.7}Hg_{0.3}Te$ QW, grown on (001) HgTe buffer for 20 nm QW width (SM phase), calculated within the 8-band $k \times p$ Hamiltonian for the Γ_6, Γ_8 and Γ_7 bands is schematically presented on Fig. 1 (see also, for example, Ref. 15).

The H1 and H2 subbands energy dispersion $E(k_\parallel)$ for a fully strained 20 nm-wide HgTe QW in $Hg_{0.35}Cd_{0.65}Te$/HgTe/$Hg_{0.35}Cd_{0.65}Te$ nanostructure is shown in Fig. 2 for the (001) orientation. We suppose that differences between the calculated (001) and experimental (013) orientations, although introduce some quantitative corrections, would not considerably influence the results of the present study. Calculations are performed in an envelope function approach within the framework of 8-band $k \times p$ theory self-consistently with the Poisson equation for the charge distribution.[11]

In the inverted regime of HgTe QW the first size-quantized heavy hole subband H1 becomes the lowest conduction band as the theory[9] predicts for it an electron-like effective mass. The highest valence band is now the second size-quantized heavy-hole subband H2 with non-monotonic dispersion law (see Fig. 1). A substantial overlap of about 6.45 meV of the valence H2 and conduction H1 subbands is obtained when the strain is considered in calculations.

3. THE LANDAU LEVEL FAN DIAGRAM

The scheme for computing $E(k_\parallel)$ was developed further for calculations of magnetic levels.[11] The magnetic levels picture for the spectrum presented in Fig. 2 is demonstrated in Fig. 3. The LL notation corresponds to the notations of Ref. 11. Here an example of the Fermi level dynamics for $n = 1.5 \cdot 10^{15}$ m^{-2} is shown for the simplest case of δ -shaped density of states in the levels.

It is seen from Fig. 3 that LL are essentially non-equidistant and nonlinearly depend on the magnetic field that is caused by the mixed nature of the H1 and H2 subbands in the inverted-band regime due to a coupling between heavy-hole to light-particle states both at finite in-plane wave vectors $k_\parallel$ (at $B = 0$)[16,17] and under the action of a magnetic field.[11]

For the H1 subband, only the lowest Landau level ($N = -2\downarrow$) contains pure heavy-hole states, which do not mix with the light-particle states[11] (see also Refs. 18–20 and references therein). It is shown in Refs. 19 and 20 that this level is of the same nature in two and in three dimensions and it is mapped on the b set level of

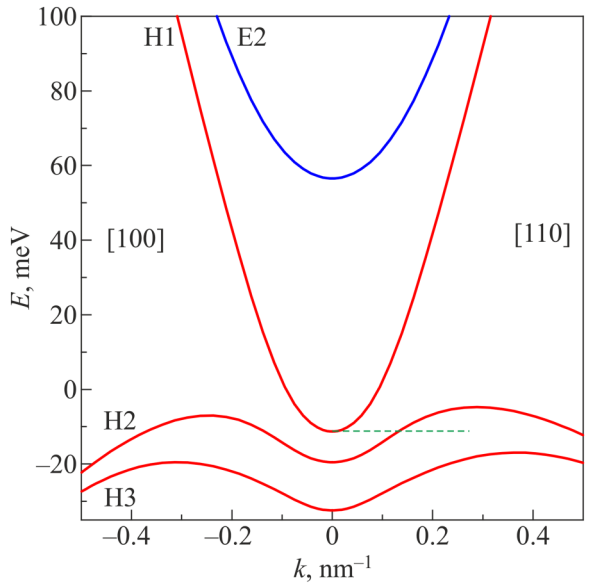

FIG. 1. The scheme of the size-quantized level layout for HgTe QW of 20 nm width. The electron-like subbands are shown in blue (E2), the red curves correspond to the heavy-hole-like subbands (H1, H2, H3).

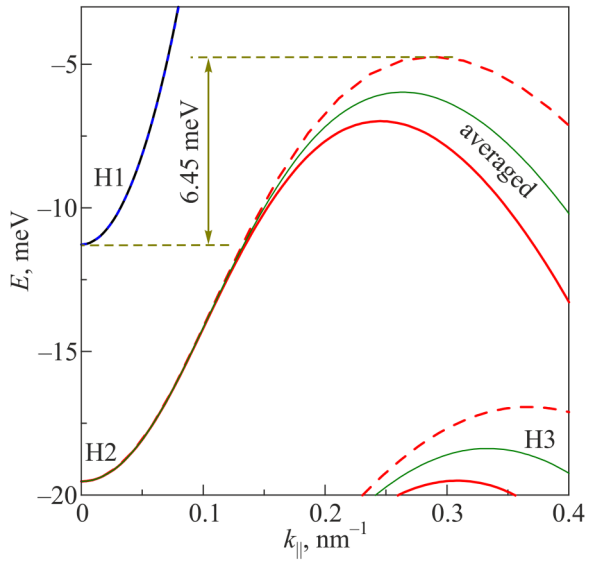

FIG. 2. The calculated band structure of a strained HgTe quantum well with $d_{QW} = 20$ nm for orientation (001): bold solid lines for $(k_x,k_y) = (1,0)$, dotted lines for $(k_x,k_y) = (1,1)$, thin solid curves for the averaged subband structure (isotropic model).

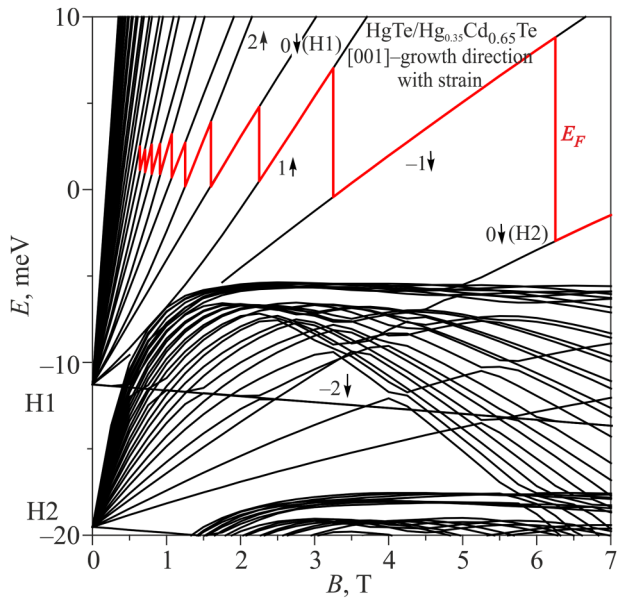

FIG. 3. Landau levels of H1 and H2 subbands for an *n*-type HgTe/$Hg_{0.3}Cd_{0.7}Te$ (001) QW as a function of the magnetic field for $d_{QW} = 20$ nm and $n = 1.5 \cdot 10^{15}$ m^{-2}. The Landau levels are labeled in accordance with the notations of Ref. 11: the quantum numbers $N = -2, -1, 0, \ldots$, and the arrows (↑,↓) indicate the dominant spin orientation of the state. The thick line represents E_F.

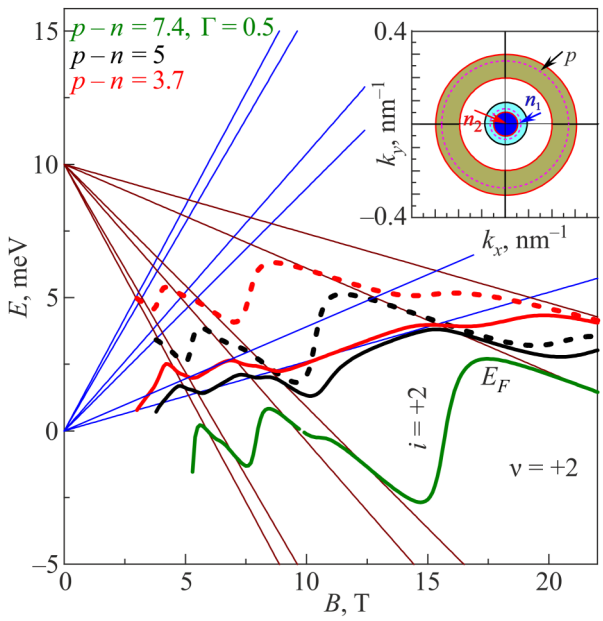

FIG. 4. Calculation of the evolution of the Fermi level in the model of the intersection of fans of the hole and electron magnetic level fan charts with a reduced hole density (*p*–*n*) (solid lines) compared to the corresponding cases without electronic levels: $n = 0$ (dashed lines). The densities shown in figure are given in 10^{15} m^{-2}. The Lorentzian shape of the density of states at the LL with a width is $\Gamma = 0.5$ meV is assumed. Inset: The corresponding Fermi contours in the (k_x; k_y) plain for the valence and conduction subbands (for the averaged energy in the valence subband so that the warping is ignored).

Guldner *et al.*:[21]

$$E_b(0) = \frac{\hbar e B}{m} \varepsilon_b(0), \tag{1}$$

where $\varepsilon_b(0) = \frac{1}{2}(\gamma_1 + \gamma - 3\kappa)$.

For the set of Γ_8 Luttinger parameters for HgTe ($\gamma_1 = 12.8$, $\gamma = 8.4$ and $\kappa = 10.5$[21]) we have

$$3\kappa > (\gamma_1 + \gamma), \tag{2}$$

and, according to (1), the level $N = -2\downarrow$ lowers its energy linearly with increasing magnetic field. All the other LL of the H1 subband rise in energy with the magnetic field due to mixing of states of heavy holes with states of light carriers induced by the magnetic field (see Ref. 11).

A nonmonotonous behavior of the main set of the H2 subband levels may be understood from a quasiclassical view for the nonmonotonic dispersion law of the valence subband with the lateral maxima, but the anomalous behavior of one the lowest magnetic level [designated as 0↓ (H2) on Fig. 3] does not have a quasiclassical interpretation.

It is a so-called zero-mode level;[22,23] it starts from the valence subband at $B = 0$ but monotonously moves up with field, as it should be for an electron level, while all the other valence subband levels, also starting from the valence subband at $B = 0$ and moving initially like electron levels, turn down later at a certain field as they reach the energy of the lateral maximum thus behaving further like the hole levels (see Fig. 3).

The unusual behavior of $N = -2\downarrow$ level from the conduction subband H1 in inverted band HgTe QWs together with the peculiar dispersion of the $N = 0\downarrow$ level from the topmost valence subband H2 leads to a crossing of conduction- and valence-subband states at some value B_c of the magnetic field (see Fig. 3). Such behavior is specific for HgTe QWs and has been examined theoretically and experimentally (see, for example, Ref. 23).

In fact, the movement of E_F is more complicated within the levels of finite width. Especially, within the field ranges where the electron and hole levels overlap, according to the modeled picture of levels in Fig. 4.

4. PRECURSIVE SCHEME FOR THE SUPERPOSITION OF ELECTRON AND HOLE LANDAU LEVELS

The specific features observed by Yakunin *et al.*[13] in magnetotransport in the double quantum well (DQW) structure built of the quasi-2D HgTe layers with the inverted energy spectrum give evidence to the overlap of the conduction and valence subbands and can be described on the basis of a calculated picture of magnetic levels in a DQW.

The coexisting electrons and holes were found in the whole investigated range of positive and negative V_g as revealed from fits to the low-field N-shaped $\rho_{xy}(B)$, from the Fourier analysis of oscillations in $\rho_{xx}(B)$ and from a specific behavior of the quantum Hall effect. The described behavior can be qualitatively explained within the framework of a simplified scheme of superposition of purely electronic and purely hole fans of LL (Fig. 4).

For the calculation of the Fermi level we simulated the finite width of the Landau levels Γ by introducing the Lorentzian shape of the density of states. The representation of the finite width of the levels allows one to display the features of the QHE (in particular, to obtain a plateau of finite dimensions), and these calculations make it possible to represent the behavior of E_F in the region of superposition of electron and hole levels.

To clarify this behavior, the calculated E_F curve for the complete set of levels (solid lines in Fig. 4) was compared with the E_F calculated for the case without electronic levels: $n = 0$, dashed lines. It can be seen that the population of electronic levels significantly changes the location of the QHE features near the intersection point of the electron and hole levels.

The empirical scheme for the overlap of the electron and hole fan diagrams of the Landau levels was also used to describe the experimental results on the quantum Hall effect near the charge neutrality point in a two-dimensional electron-hole system of a 20.5 nm HgTe quantum well by Gusev *et al.*[12]

5. QUASICLASSICAL CALCULATION OF THE LANDAU LEVEL SPECTRUM ("EXTREMUM LOOP" MODEL)

We use a semiclassical approach to calculate the effective mass and the LL spectrum of the valence band, based on the known dispersion law, $E(k_x, k_y)$, of the H2 subband (see Fig. 2). Physically, we will assume that the appearance of holes in the valence band, completely filled by the electrons, begins from the tops of the H2 subband, which are at its lateral maxima. We get a set of isoenergetic trajectories, sequentially cutting off the dependence $E(k_x, k_y)$ by the planes $\varepsilon = \text{const}$, starting from $\varepsilon = 0$ at the tops of the lateral maxima.

For the calculation in the isotropic approximation, the so-called "extremum loop" model used when the extremum (in our case maximum) of the electron energy is achieved not at separate isolated points, but on a whole closed curve in momentum space.[24,25]

5.1. Isotropic approximation

Figure 5(a) shows the band structure of a strained HgTe quantum well with $d_{QW} = 20$ nm in the isotropic approximation when the corrugation of zone Γ_8 is not taken into account.[11,13] Fig. 5(b) shows the isoenergetic contours of the bottom of the conduction band (small circle centered at a point Γ) and of the top of the valence band [circles with radii $(k_0 \pm \Delta k)$ in coordinates (k_x, k_y)] corresponding to energy ε [dashed line in Fig. 5(a)].

In the isotropic approximation, the isoenergetic contours near the top of the valence band have the form of rings [see Fig. 5(b)], and we use the model proposed in Ref. 24 for semi-conductors with a wurtzite lattice to calculate the effective mass and the LL spectrum of holes. Rashba and Sheka[24] showed that if we neglect

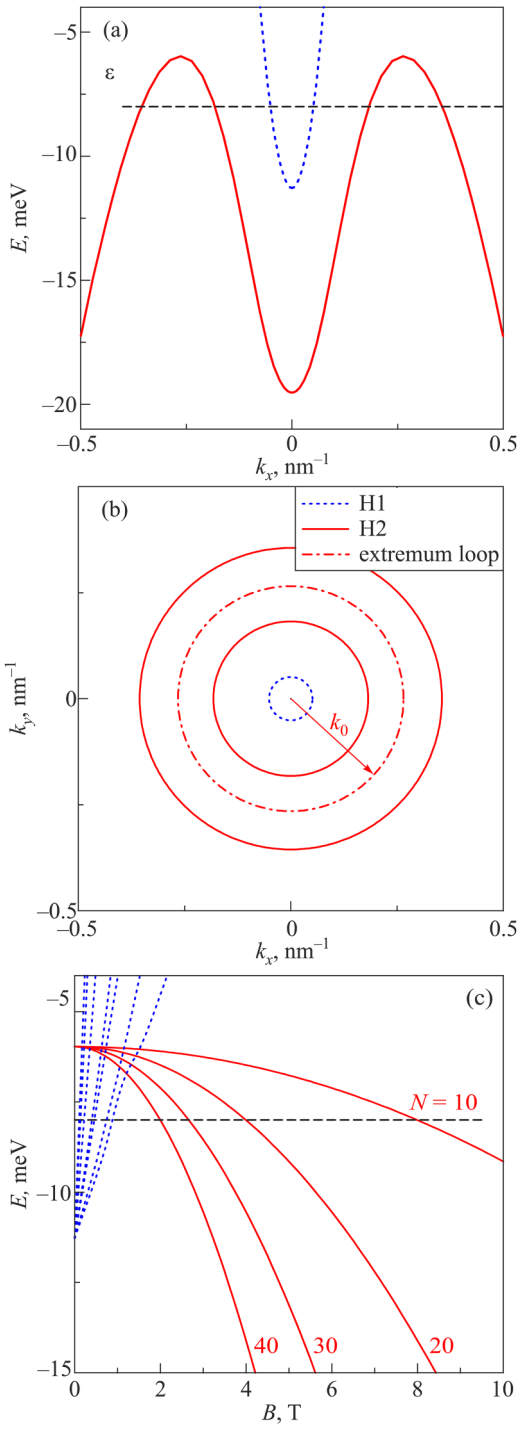

FIG. 5. (a) Band structure of a strained HgTe quantum well with $d_{QW} = 20$ nm in the isotropic approximation. (b) Isoenergetic contours of the bottom of the conduction band and the top of the valence band in coordinates (k_x, k_y), corresponding to the energy ε [dashed line in Fig. 5(a)]. (c) The spectrum of the Landau levels of the valence band, calculated in the "extremum loop" model.

the anisotropy of relativistic interactions, then the minimum of the electron energy in these semiconductors is achieved not at separate isolated points of momentum space, but on a whole curve—a circle, which was called a "loop of extrema".

In this model for the 2D case, the dispersion law of holes with energies close to extremum (at $p_\perp = p_0 \equiv \hbar k_0$), when calculating the energy to the valence-band depth, may be taken in the form

$$\varepsilon = \frac{1}{m_a}(p_\perp - p_0)^2, \tag{3}$$

with $p_\perp = (p_x^2 + p_y^2)^{1/2}$ and m_a being the curvature of the side parabola vertex in the Fig. 2.

In the semiclassical approximation[26] for the effective cyclotron mass we have

$$m_c(\varepsilon) = \frac{1}{2\pi}\frac{dS(\varepsilon)}{d\varepsilon} = p_0\sqrt{\frac{2m_a}{\varepsilon}} = 2m_a\sqrt{\frac{\varepsilon_a}{\varepsilon}}, \tag{4}$$

with

$$\varepsilon_a = \frac{p_0^2}{2m_a},$$

where $S(\varepsilon) = 4\pi p_0\sqrt{2m_a\varepsilon}$ is the area of the ring cut off from the lateral maximum in the valence band by the plane of constant energy, depicted in Fig. 5(b).

It is seen that cyclotron effective mass diverges when approaching the top of the valence band as $1/\sqrt{\varepsilon}$. The analysis of the features of the semiclassical effective mass of carriers in crystals of the wurtzite type is done in the work of Yermolaev.[25]

For the distance between energy levels quantized by magnetic field B (cyclotron energy) we have

$$\hbar\omega_c = \frac{\hbar eB}{m_c(\varepsilon)} = \hbar\omega_a\sqrt{\frac{\varepsilon}{\varepsilon_a}} \text{ with } \omega_a = \frac{eB}{m_a}. \tag{5}$$

The energy of the Nth Landau level (at $N \gg 1$) is determined by the expression $\varepsilon = N\hbar\omega_c$ and taking into account the dependence $m_c(\varepsilon)$, for the LL spectrum of holes in the QW HgTe valence band in the "extremum loop" model we finally find

$$\varepsilon(N, B) = \frac{(N\hbar\omega_a)^2}{4\varepsilon_a}, \text{ i.e., } \varepsilon(N, B) \sim N^2B^2. \tag{6}$$

The spectrum of the LL of the valence band, calculated in the "extremum loop" model, is schematically shown in Fig. 5(c). It is important that this LL fan starts with energy $\varepsilon = 0$, corresponding to the energy of the tops (side maxima) of the valence band (H2 subband) and overlaps with the LL fan of the conduction band (H1 subband), as it should be in the SM phase.

5.2. Effects of cubic symmetry in hole spectrum

Taking into account anisotropy, in accordance with Fig. 2, leads to a more complex form of isoenergetic contours near the top of the H2 subband (see, for example, Ref. 27). The pattern of the constant energy lines of the valence band, taking into account the corrugation, is shown in Fig. 6(a): at low energies, the ground states of holes become four maxima displaced from the center of the Brillouin zone in directions (±1; ±1), and there are four saddle points in directions (0; ±1) and (±1; 0).

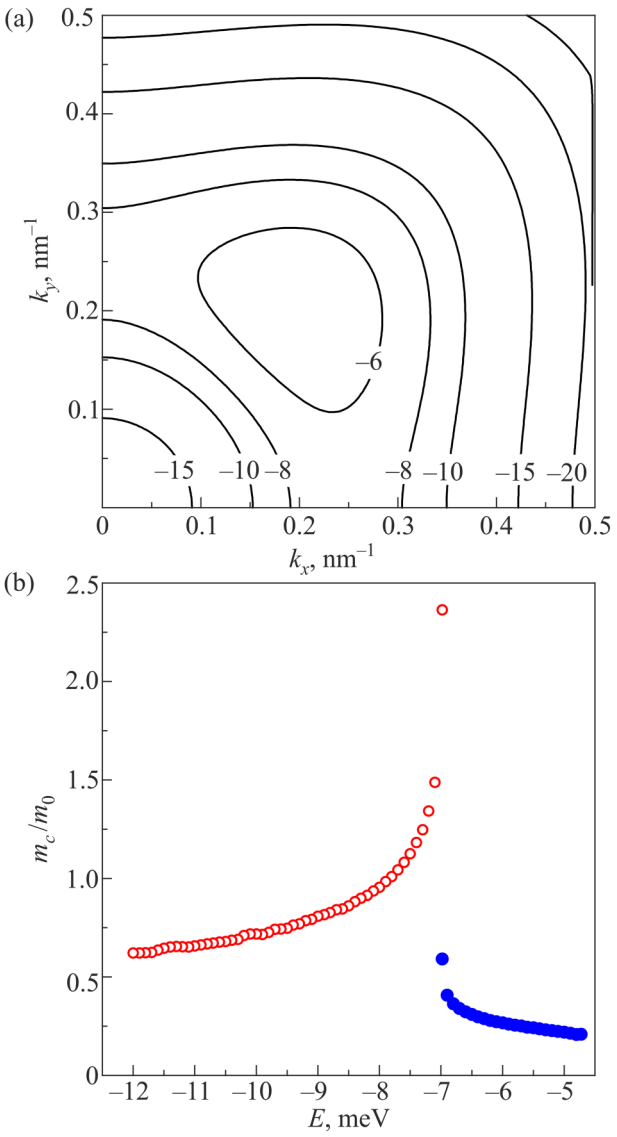

FIG. 6. (a) The pattern of constant energy contours near the top of the H2 subband with allowance for the corrugation of the hole spectrum. Only one quadrant of the Brillouin zone is shown. The numbers on the curves correspond to the values of the energy ε (meV) measured from the top of the lateral maximum of the valence band. (b) Dependence of the effective mass on energy with the corrugation effects in the hole spectrum. It is taken into account that the states above the saddle point (open points) are four-fold degenerate.

Indeed, multiple intersections of the Fermi level with nonmonotonic energy spectrum (Fig. 2) lead to a complicated Fermi surface for 2D electrons (Fermi arc) composed of more than one closed branches providing both electron-like and hole-like orbits in the presence of the perpendicular magnetic field.[28]

At energies below the saddle points, the isoenergetic contours take the form of deformed ("crimped") rings, and we again have an "extremum loop" when the maxima of the hole energy are reached on a smooth closed curve in momentum space [see Fig. 3(b) in Ref. 29].

Figure 6(b) shows the dependence of the cyclotron effective mass on the energy, $m_c(\varepsilon)$, taking into account the effects of cubic symmetry. On the whole, the corrugation effect leads to an anomalous dependence of $m_c(\varepsilon)$ with a logarithmic divergence at the saddle points and, as a consequence, to a complex form of the LL pattern. At energies above the saddle point [open dots in Fig. 6(b)], these values of the effective cyclotron mass m_c correspond to a fourfold degenerate (without taking spin into account) state. Below the saddle point, the values m_c of the effective cyclotron mass behaves similarly to the case in the case of the extremum loop model.

Generally, the quasiclassical approach provides a quantitative ground for the empirical Landau level scheme of HgTe QW in the SM phase (see Fig. 4). On the other hand, in quantum-mechanical calculations, the "electronic" part of the LL of the H2 subband (at $B < 2T$ in Fig. 3) is formally obtained due to the additional (with respect to mix at finite $k_{\|}$ for $B = 0$) mixing of the states of heavy holes with states of light carriers, induced by a magnetic field.

If we proceed from the dispersion law in Fig. 2, this part of the Landau level system is in the forbidden band of the semiconductor. So additional consideration of the form of the magnetic level spectrum for H2 subband, from the point of view of the completely filled valence band, seems necessary.

6. CONCLUSIONS

This work is devoted to the analysis of the spectrum of the valence band in HgTe QW with an inverted band structure, which is formed by the states of the size-quantized H2 subband of heavy holes with a nonmonotonic dispersion law. A brief overview of the concepts of the dispersion law at $B = 0$, as well as of the available phenomenological models and quantum-mechanical calculations of the Landau level spectrum for the HgTe QW in the semimetallic phase is given.

The effective mass and the Landau level spectrum for H2 subband are calculated in the quasiclassical "extremum loop» model. Under this model, in the semimetallic phase, the fan of Landau levels in the valence band starts at $B = 0$ with an energy corresponding to the energy of the side maxima of this band and overlaps with the fan of Landau levels in the conduction band.

The correspondence of quantum-mechanical calculations of the Landau levels spectrum[11,13] with the semiclassical picture, considered in this article, was analyzed in the report of Yakunin *et al.*[30] Note that the semiclassical approach is important for the theoretical estimation of the effective mass of holes in a complex valence band with a nonmonotonic dispersion law.

ACKNOWLEDGMENTS

The research was carried out within the state assignment of Ministry of Science and Higher Education of the Russian Federation (theme "Electron" No. AAAA-A18-118020190098-5), supported in part by RFBR, Project No. 18-02-00172. We are grateful to Novik E. G. for the contribution to the band structure calculations of the real 20 nm HgTe quantum well.

REFERENCES

[1]M. König, H. Buhmann, L. W. Molenkamp, T. Hughes, C.-X. Liu, X.-L. Qi, and S.-C. Zhang, J. Phys. Soc. Jpn. **77**, 031007 (2008).
[2]Z. D. Kvon, E. B. Olshanetsky, N. N. Mikhailov, and D. A. Kozlov, Fiz. Nizk. Temp. **35**, 10 (2009) [Low Temp. Phys. **35**, 6 (2009)].
[3]B. A. Bernevig, T. L. Hughes, and S.-C. Zhang, Science **314**, 1757 (2006).
[4]M. König, S. Wiedmann, C. Brüne, A. Roth, H. Buhmann, L. W. Molenkamp, X.-L. Qi, and S.-C. Zhang, Science **318**, 766 (2007).
[5]S. S. Krishtopenko, I. Yahniuk, D. B. But, V. I. Gavrilenko, W. Knap, and F. Teppe, Phys. Rev. B **94**, 245402 (2016).
[6]Z. D. Kvon, E. B. Olshanetsky, D. A. Kozlov, N. N. Mikhailov, and S. A. Dvoretskii, Pisma Zh. Eksp. Teor. Fiz. **87**, 588 (2008) [JETP Lett. **87**, 502 (2008)].
[7]Z. D. Kvon, E. B. Olshanetsky, E. G. Novik, D. A. Kozlov, N. N. Mikhailov, I. O. Parm, and S. A. Dvoretsky, Phys. Rev. B **83**, 193304 (2011).
[8]E. B. Olshanetsky, Z. D. Kvon, N. N. Mikhailov, E. G. Novik, I. O. Parm, and S. A. Dvoretsky, Solid State Commun. **152**, 265 (2012).
[9]M. I. D'yakonov and A. V. Khaetskii, JETP **55**, 917 (1982), available at http://www.jetp.ac.ru/cgi-bin/dn/e_055_05_0917.pdf.
[10]C. Brüne, C. X. Liu, E. G. Novik, E. M. Hankiewicz, H. Buhmann, Y. L. Chen, X. L. Qi, Z. X. Shen, S. C. Zhang, and L. W. Molenkamp, Phys. Rev. Lett. **106**, 126803 (2011).
[11]E. G. Novik, A. Pfeuffer-Jeschke, T. Jungwirth, V. Latussek, C. R. Becker, G. Landwehr, H. Buhmann, and L. W. Molenkamp, Phys. Rev. B **72**, 035321 (2005).
[12]G. M. Gusev, E. B. Olshanetsky, Z. D. Kvon, N. N. Mikhailov, S. A. Dvoretsky, and J. C. Portal, Phys. Rev. Lett. **104**, 166401 (2010), cond-mat. 1003.5908.
[13]M. V. Yakunin, A. V. Suslov, M. R. Popov, E. G. Novik, S. A. Dvoretsky, and N. N. Mikhailov, Phys. Rev. B **93**, 085308 (2016).
[14]G. M. Minkov, V. Y. Aleshkin, O. E. Rut, A. A. Sherstobitov, A. V. Germanenko, S. A. Dvoretski, and N. N. Mikhailov, Phys. Rev. B **96**, 035310 (2017).
[15]S. S. Krishtopenko, I. Yahniuk, D. B. But, V. I. Gavrilenko, W. Knap, and F. Teppe, Suppl. Mater. Phys. Rev. B **94**, 245402 (2016).
[16]T. Wimbauer, K. Oettinger, A. L. Efros, B. K. Meyer, and H. Brugger, Phys. Rev. B **50**, 8889 (1994).
[17]M. A. Semina and R. A. Suris, Semiconductors **49**, 797 (2015).
[18]S. V. Gudina, V. N. Neverov, E. G. Novik, E. V. Ilchenko, G. I. Harus, N. G. Shelushinina, S. M. Podgornykh, M. V. Yakunin, N. N. Mikhailov, and S. A. Dvoretsky, Fiz. Nizk. Temp. **43**, 605 (2017) [Low Temp. Phys. **43**, 485 (2017)].
[19]Y. G. Arapov, N. A. Gorodilov, V. N. Neverov, M. V. Yakunin, A. V. Germanenko, G. M. Min'kov, O. A. Kuznetsov, R. A. Rubtsova, A. L. Chernov, and L. K. Orlov, JETP Lett. **59**, 245 (1994), see http://www.jetpletters.ac.ru/ps/1298/article_19604.shtml.
[20]M. V. Yakunin, G. A. Alshanskii, Y. G. Arapov, G. I. Harus, V. N. Neverov, N. G. Shelushinina, and O. A. Kuznetsov, Nanotechnology **11**, 351 (2000).
[21]Y. Guldner, C. Rigaux, M. Grynberg, and A. Mycielski, Phys. Rev. B **8**, 3875 (1973).
[22]F. Ancilotto, A. Fasolino, and J. C. Maan, Phys. Rev. B **38**, 1788 (1988).
[23]M. Schultz, U. Merkt, A. Sonntag, U. Rössler, R. Winkler, T. Colin, P. Helgesen, T. Skauli, and S. Løvold, Phys. Rev. B **57**, 14772 (1998).
[24]E. I. Rashba and V. I. Sheka, Sov. Phys. Solid State **1**, 143 (1959).
[25]A. M. Yermolaev, Sov. Phys. Solid State **8**, 560 (1966).
[26]I. M. Lifshits, M. Y. Azbel', and M. I. Kaganov, *Electron Theory of Metals* (Nauka, Moscow, 1971).

[27]G. Landwehr, J. Gerschutz, S. Oehling, A. Pfeuffer-Jeschke, V. Latussek, and C. R. Becker, Physica E **6**, 713 (2000).
[28]O. E. Raichev, G. M. Gusev, E. B. Olshanetsky, Z. D. Kvon, N. N. Mikhailov, S. A. Dvoretsky, and J. C. Portal, Phys. Rev. B **86**, 155320 (2012), cond-mat 1210.7219.
[29]S. V. Gudina, A. S. Bogolyubskii, V. N. Neverov, N. G. Shelushinina, and M. V. Yakunin, Semiconductors **52**, 1404 (2018).
[30]M. V. Yakunin, S. M. Podgornykh, M. R. Popov, S. S. Krishtopenko, F. Teppe, B. Jouault, W. Desrat, N. N. Mikhailov, and S. A. Dvoretskii, in *Proceedings of the 22nd Ural International Winter School on Semiconductor Physics* (Ekaterinburg, Russia, 2018), p. 170.

Translated by AIP Author Services